Ene/Diene Copolymerization Catalyzed by Cationic Sc and Gd d 0 Metal Complexes: Speciation, Ion Pairing, and Selectivity from a Computational Perspective

Ludmilla Verrieux, Julien Thuilliez, François Jean-Baptiste-Dit-Dominique, Christophe Boisson, Marie-Noëlle Poradowski, Lionel Perrin

Ene / diene (co)polymerization catalyzed by cationic Sc and Gd d^0 metal complexes: speciation, ion pairing and selectivity from a computational perspective

Ludmilla Verrieux,[a,b] Julien Thuilliez,[b] François Jean-Baptiste-dit-Dominique,[b] Christophe Boisson,[c] Marie-Noëlle Poradowski,[a,b] and Lionel Perrin*[a]*

[a] Université de Lyon, Université Claude Bernard Lyon I, CNRS, INSA, CPE, UMR 5246, ICBMS, 1 rue Victor Grignard, F-69622 Villeurbanne cedex, France

[b] Manufacture Michelin, 23 pl Carmes Déchaux, F-63000 Clermont-Ferrand, France

[c] Université de Lyon, Université Claude Bernard Lyon 1, CPE Lyon, CNRS, UMR 5265, Chemistry, Catalysis, Polymers and Processes (C2P2), 43 Bd du 11 Novembre 1918, 69616 Villeurbanne, France

metallocene • d^0 metal complexes • butadiene • polymerization • speciation • ion pairing • reactivity • DFT

ABSTRACT A computational mechanistic study of the butadiene homopolymerization reaction performed with scandium and gadolinium catalysts $[(2\text{-Me-Ind})_2(N(TMS)_2)]M$ (M = Sc, Gd) in presence of $[Ph_3C][B(C_6F_5)_4]$ or $[PhNMe_2H][B(C_6F_5)_4]$ and Al_2Et_6 has been performed at the DFT level. The speciation of mono- and poly-metallic complexes involving alkylaluminum and the cationizing agent has been achieved. Their dormant or active character has been revealed. This speciation shows a thermodynamically favorable transmetalation reaction between the aryl group of $[B(C_6F_5)_4]^-$ and the alkyl group of AlR_3. The reactivity of $[(2\text{-Me-Ind})(Et)M]^+$ (M = Gd, Sc) toward monomer insertions is detailed. Computed energy profiles demonstrate the preference for *cis*-1,4 over *trans*-1,4 insertion. The influence of the counter-ion on the reactivity and selectivity of the catalyst has been investigated. For Gd-based system, the counter-ion has an impact on the reactivity and selectivity of the catalyst and cannot be omitted in the chemical model. Finally, the ability of these cationic complexes to copolymerize ethylene with butadiene is assessed and compared to neutral and efficient Nd based catalytic systems.

INTRODUCTION

Since the discovery of Ziegler-Natta catalysts in the 1950s, many catalytic systems have been developed for olefins and dienes homo- and co-polymerization. These polymers are present in our daily lives and their synthesis and properties currently meet new challenges like recyclability, raw-material economy and low carbon footprint.[1,2] For those purposes, researchers are aiming to develop new catalysts with high activities and high control of polymer microstructures. Since the 1960s, catalytic systems mainly based on group 3 or group 4 metals and lanthanides were designed and elaborated. Interestingly, the control of the microstructure of synthesized polymers conferred

by these catalytic systems can still be enhanced by the fine adjustment of the structure of the (pre)catalysts and the usage conditions of the catalytic mixture.[1,3]

In this context, several organometallic catalysts for butadiene polymerization have been developed to obtain synthetic Butadiene Rubbers (BR) that are of particular interest for the tire industry. The development of stereocontrolled butadiene homopolymerization catalysts is peculiarly appealing and challenging as synthetic BR properties strongly depend on polybutadiene microstructures.[4] For example, a high content of *cis*-1,4 units increases elastomeric properties that confer better abrasion and fatigue resistance or a higher resilience to the material.[4,5,6] Efficient catalytic systems are mainly based on cobalt, nickel, titanium and neodymium.[4] The latter provide linear polymers with a quasi-regular *cis*-1,4 content[1,5] whereas cobalt based catalysts yield branched frameworks.[5] Interestingly, it has been shown that rare earth metallocene complexes, when associated to a cationizing agent like $[Ph_3C][B(C_6F_5)_4]$ and a cocatalyst such as $(AlR_3)_n$ or $(MgR_2)_n$, yield half-sandwich cationic species that are much more active than neutral ones towards butadiene polymerization.[1,3,6] For example, Wakatsuki and coworkers have characterized the cation $[(C_5Me_5)_2Ln]^+$ (Ln = Pr, Nd)[7] and have reported the activity of $[(C_5Me_5)_2Ln]^+$ (Ln = Pr, Nd, Sm, Gd) towards *cis*-1,4-butadiene polymerization in the presence of alkylaluminum.[7,8,9] Similarly, Tardif et al. have reported the structure of $[(2\text{-R-Ind})Ln(N(TMS)_2)(L)_n]^+$ (Ln = Sc, Gd; L = THF and n = 2, L = $PhNMe_2$ and n = 1) complexes and their activity towards *cis*-1,4-butadiene polymerization in the presence of alkylaluminum.[6] Regarding the complexity of the catalytic mixtures mentioned above, the molecular structure of both dormant and active species is questioned in most experimental studies that aim to relate catalyst activities and selectivities to catalyst components. From these experimental studies, putative structures of the active species are most often suggested or inferred.

Several communications raised this interrogation and mentioned that different polymetallic species can be formed between the activated precursor and alkyl reagents.[10,11,12] For example, in a joint theoretical / experimental study, Ehm et al. have reported the characterization by NMR spectroscopy of polymetallic edifices between zirconocene complexes and trimethylaluminium (TMA) depending on the concentration of TMA.[10] Calculations carried out at the DFT level have justified that the formation of the heterobimetallic complexes highlighted in Scheme 1 is thermodynamically favorable relative to mixed reagents. In a recent and joint theoretical / experimental study, the group of Zuccaccia in collaboration with the Dow Chemical Company has reported the characterization of cationic bridged Hf-Al and Hf-Zn heterobimetallic complexes and has highlighted the role played by agostic interactions in stabilizing the complexes.[13]

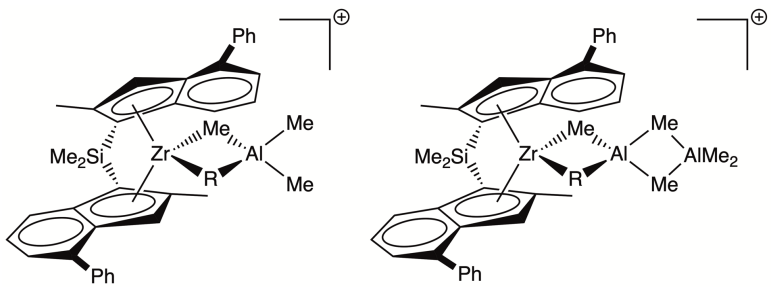

Scheme 1. Stable adducts formed between cationic *ansa*-zirconocene complexes and trimethylaluminium (TMA).[10]

Mathis et al. have not only investigated the speciation between Zr and Al based compounds, but they more specifically focused on the transmetalation reaction between boron-C_6F_5 compounds ($B(C_6F_5)_3$ or $[Ph_3C][B(C_6F_5)_4]$) and Al_2R_6. Different aggregation modes between $B(C_6F_5)_3$ and trialkylaluminum were thus characterized during the activation of zirconium complexes.

Depending on B:Al ratio, two heterobimetallic species were depicted and characterized, Scheme 2.[12]

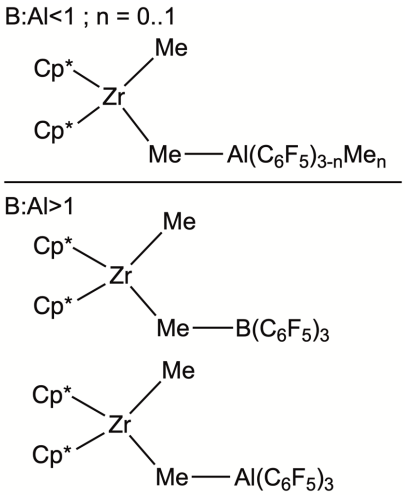

Scheme 2. Representative zirconium complexes formed, as observed by NMR spectroscopy, upon exchange reactions between boron fluoroaryl compound $B(C_6F_5)_3$ and alkylaluminum species Al_2R_6, Cp* = C_5Me_5.[12]

If AlR_3 is in excess relative to boron fluoroaryl compound $B(C_6F_5)_3$, a consequence of the transmetalation is the formation of the Zr/Al bimetallic complex in which aluminum supports two or three fluoroaryl groups. If boron fluoroaryl compound $B(C_6F_5)_3$ is in excess relative to AlR_3, a mixture of Zr/Al and Zr/B in which aluminum or boron supports three fluoroaryl groups has been characterized. This illustrates the efficiency of the Al / B transmetalation reaction. As the counter-ion ensures the stability of the ion pair, its spectator or actor character towards the reactivity, and more specifically the selectivity, of catalytic systems is questioned. Several studies suggest that during olefins polymerization, the approach of the monomer towards the metal center expels the counter-ion from the inner-sphere to the outer-sphere and consequently that this latter has thus a

minor influence on computed energy barriers once the catalyst is activated and if the counter-ion does not support a Me group (Figure 1).[14,15,16,17] The influence of ion-pairing on the activity and selectivity of diene polymerization has thus motivated our detailed computational investigation.

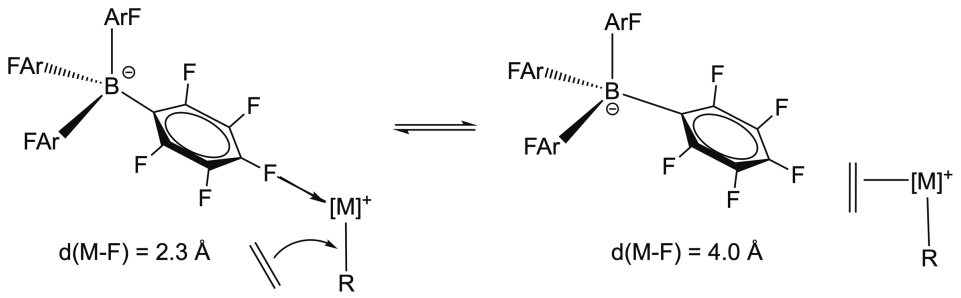

Figure 1. Mechanism of first coordination sphere counter-ion displacement induced by monomer coordination (ArF = C_6F_5; M = Hf, Zr, Ti).[14,15,16,17]

In the present communication, we focused on the mechanistic investigation of the catalytic systems developed by Tardif[6] who synthetized both scandium and gadolinium metallocene complexes supported by one silylamido group and two indenyl ligands substituted in position 2. When engaged in butadiene polymerization in presence of a cationic agent ($[PhNHMe_2][B(C_6F_5)_4]$ or $[Ph_3C][B(C_6F_5)_4]$) and iBu$_3$Al as an alkylating agent, the catalytic system proved to be selective towards *cis*-1,4 units (Scheme 3).[6] The major question raised by this polymerization reactions concerns the determination of the active species and subsequently the dormant ones by considering the interactions between the alkylaluminum, the cationizing agent and the Sc- or Gd-based precursors towards the selectivity of butadiene insertion. A second aim, is to assess the ability of such catalytic system to copolymerize ethylene with butadiene for the synthesis of ethylene butadiene copolymers.

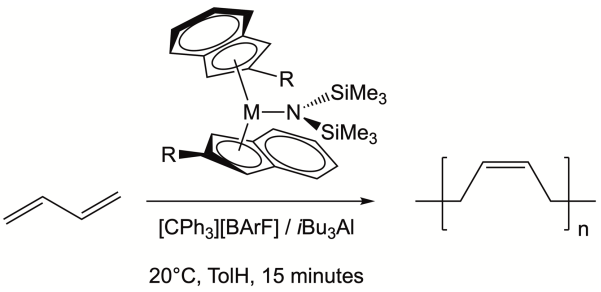

Scheme 3. Butadiene polymerization reaction with bis(indenyl) amido metallocene complexes (M = Sc or Gd; R = H, Me or Ph).[6]

After a presentation of the modelling strategy and of the level of calculation, we address the speciation of the catalytic system $(Ind')_2M(N(TMS)_2)$ (M = Sc, Gd; Ind' = 2-substituded indenyl, TMS = $SiMe_3$) in presence of the cationizing agent and alkylaluminum. Then energy profiles for monomer insertions is presented, and the impact of the counter-ion on the reactivity is discussed. Finally, of the ability of the active species to perform the copolymerization of butadiene with ethylene is assessed computationally.

MODELLING STRATEGY AND COMPUTATIONNAL DETAILS

Since this computational study involves d^0 metal complexes based on scandium (*d*-block) and gadolinium (*f*-block), Relativistic Electron Core Potentials (RECPs) were used.[18] In this approach, only valence electrons are explicitly represented, the influence of core electrons on the valence are represented by a potential. As the oxidation state of Gd and hence the 4*f* population do not change during the polymerization reaction, a large core RECP (53 electron in core) adapted to the +III oxidation state was used,[18,19,20,21] in combination with its associated basis sets augmented by a *f* function (ζ = 1,0).[22,23] This approximation is reasonable as the 4*f* electrons have a neglectable contribution in the metal–ligand bonding picture.[19,21] Scandium was described by a 10 electrons

full-relativistic Stuttgart-Cologne RECP and its associated polarized basis set.[22,23] Silicon was represented by a 10 electrons Stuttgart-Koln relativistic pseudopotential and its associated basis sets.[24] For C, H, F, B, and N atoms, the polarized all-electron triple-ζ 6-311G(*d,p*) basis sets were used.[25] Aluminum was described by the augmented 6-311++G(*d,p*) basis set[25,26] that enables a proper depiction of the structural diversity of alkylaluminum clusters.[27,28] Concerning the choice of the density functional, it has been shown that the hybrid functional B3PW91[29,30] allows to obtain a good comprise between accuracy and cost of the calculations.[31,32,33] Solvation by toluene was modeled during optimization by an implicit model (SMD-toluene),[34] when THF is used as a co-solvent, explicit THF molecules were added to the model in order to complete the coordination sphere of the metal. Dispersion contributions were added by means of a single-point correction using the damped empirical Grimme D3-BJ correction.[35,36,37] Energy values correspond to Gibbs energy given in kcal mol^{-1} estimated at 298 K and 1 atm. Enthalpy and entropy contributions are estimated within the harmonic oscillator approximation. All calculations were performed with Gaussian 09 revision D01.[38] Geometry optimization of the reactants and transition states were performed without any symmetry restrictions or geometrical constraints. The nature of extrema (minimum or transition state) was verified by analytical frequency calculation. The connectivity of each transition state has been checked by following the Intrinsic Reaction Coordinate of each transition state. Conformational sampling has been performed by hand. Only the most stable conformers are presented. The exhaustivity of the sampling is presented as a supporting information (see ESI). Finally, as a chemical model, experimental Sc and Gd-based complexes were fully represented without any structural simplification. The polymer chain is depicted by at least by an ethyl group in order to avoid artefacts.[39]

RESULTS AND DISCUSSION

Notations. First, ^{Sc} and ^{Gd} are respectively used as prefix tags for scandium and gadolinium based complexes, except for the cationic complex $[(2\text{-Me-Ind})(Et)M]^+$ which is noted $[M]^+$ (M = Sc, Gd). Additional notations are used to define insertion sequences. As the primary insertion of butadiene yields an alkyl site while the secondary insertion forms an allyl site, the four different modes of insertion of butadiene are noted: *trans* primary (^{12T}B), *cis* primary (^{12C}B), *trans* secondary (^{14T}B) and *cis* secondary (^{14C}B). Additionally, at an allyl site M(η^3-RC_3H_4), insertion can either occur at the central M-C^3 bond of the allyl group, leading to a ^{21C}B unit, or at the terminal M-C^1 bond yielding to a ^{14C}B unit. Furthermore, two additional monomer approaches originate from the asymmetry of the substituted indenyl ligand. These two approaches are differentiated as depicted in Scheme 4. Notation *r* corresponds to a monomer approaching on the side of the indenyl substituent. Notation *l* corresponds to a monomer arriving on the side of the indenyl benzene ring. Transition state are quoted with an asterisk mark after the inserted monomer (eg ^{12C}B^{12C}B*), monomer adducts to an active site are noted with an underscore character (eg ^{12C}B_^{12C}B). Neutral ion pairs in which the counter-ion is explicitly considered in the chemical model are labelled by the suffix ° (eg ^{12C}B_^{12C}B°).

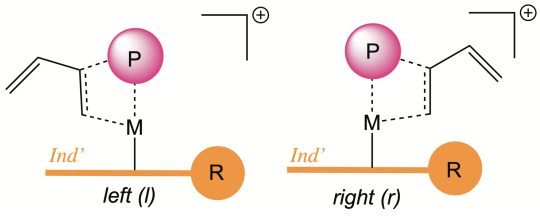

Scheme 4. Definition of *left* / *right* notations (in orange: indenyl ligand, in pink: polymer chain noted P).

Speciation. *Dimer monomer equilibrium of triethylaluminum (TEA)*. In order to establish a common and global energy reference, the most stable form of each species present in the catalytic solution were defined. The mechanisms that relate all the species considered have not been investigated and the associated kinetics is assumed to be fast and not determinant. In order to avoid the extensive sampling of the conformational space originating from the *i*Bu groups of triisobutylaluminium (TIBA), TIBA was modelled by TEA though the steric hindrance of the isobutyl groups significantly hampers aggregation.[40] Based on previously reported speciation of trimethylaluminum (TMA),[41,42] one monomer and two types of dimer were optimized. Monomer $\mathbf{Al_1}$ has a trigonal plane geometry, dimers $\mathbf{Al_2}^{cis}$ and $\mathbf{Al_2}^{trans}$ display respectively *cis*- or *trans*-periplanar alkyl bridges (Scheme 5). Isomer $\mathbf{Al_2}^{trans}$ is the most thermodynamically stable. The dimerization of $\mathbf{Al_1}$ in $\mathbf{Al_2}^{trans}$ is computed exergonic by 9.1 kcal mol^{-1} that is in fair agreement with the experimental Gibbs energy value of 7.4 kcal mol^{-1} estimated at 298 K.[43] Optimization attempts of clusters with a higher degree of aggregation turned out to be dissociative. This is in line, so far, with the absence of characterization of larger aggregates,[44,45] and the bonding picture of alkylaluminum compounds.[46]

Determination of dormant and active species. The cationic species reported by Tardif et al. are obtained after the activation of the bis-indenyl-silylamido Sc neutral complex $^{Sc}\mathbf{1}$ by $[CPh_3]^+$ or $[PhNHMe_2]^+$ borate salts. For the sake of clarity, results are presented with $[CPh_3][BArF]$ ($[BArF]^- = [B(C_6F_5)_4]^-$) as a cationizing agent but very similar trends were computed with the anilinium salt $[PhNHMe_2][BArF]$ (see Scheme S1).

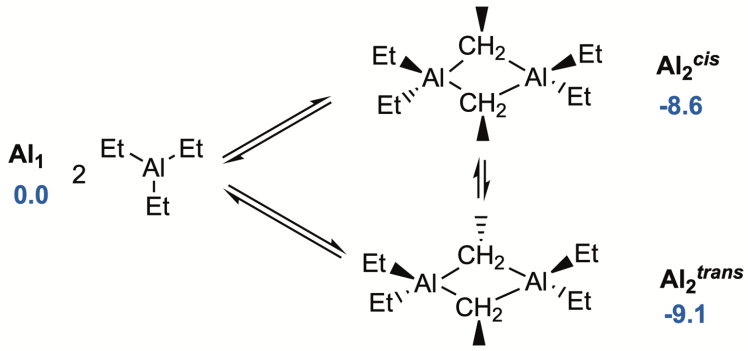

Scheme 5. Optimized isomers of TEA and their relative Gibbs energies in kcal mol^{-1}.

Though the cationic mono-indenyl species ^{Sc}**2** and ^{Sc}**4** (Scheme S1 and 6) were synthesized and characterized by X-ray diffraction analysis, we have also considered a pathway in which the cationic bis(indenyl) species ^{Sc}**3** is formed resulting from the abstraction of the amido group by the trityl cation (Scheme S1 and 6). In the presence of THF, the formation of cationic complex ^{Sc}**2** is exergonic by 15.5 kcal mol^{-1} due to the coordination to the metal center of two tetrahydrofuran (THF) solvent molecules. This pathway is thermodynamically the most favorable. In absence of THF, the cationization of precursor ^{Sc}**1** into complex ^{Sc}**4** remains exergonic by 5.2 kcal mol^{-1} (Scheme 6). The abstraction of the indenyl group is computed more favorable than the displacement of the bis-silylamido ligand by 2.1 kcal mol^{-1}. This thermodynamic trend agrees with experimental results[6] and brings confidence in the computational strategy. In order to pinpoint catalytically active species, all the possible alkylation reaction of complexes ^{Sc}**2** and ^{Sc}**4** were considered. The first hypothesis is the formation of monometallic alkylated species, free of TEA. In this case, alkylation can proceed via the displacement of the amido or the indenyl ligands of ^{Sc}**4**. The displacement of the silylamido group by an alkyl group to yield ^{Sc}**5a** is almost thermoneutral, and thermodynamically more favorable than the displacement of the indenyl ligand by 23.5 kcal mol^{-1} (see Scheme S1). Finally, polyalkylations of complex ^{Sc}**4** have also been investigated and

turned out to be unrealistic with computed endergonicity higher than 30 kcal mol^{-1} (see Scheme S2).

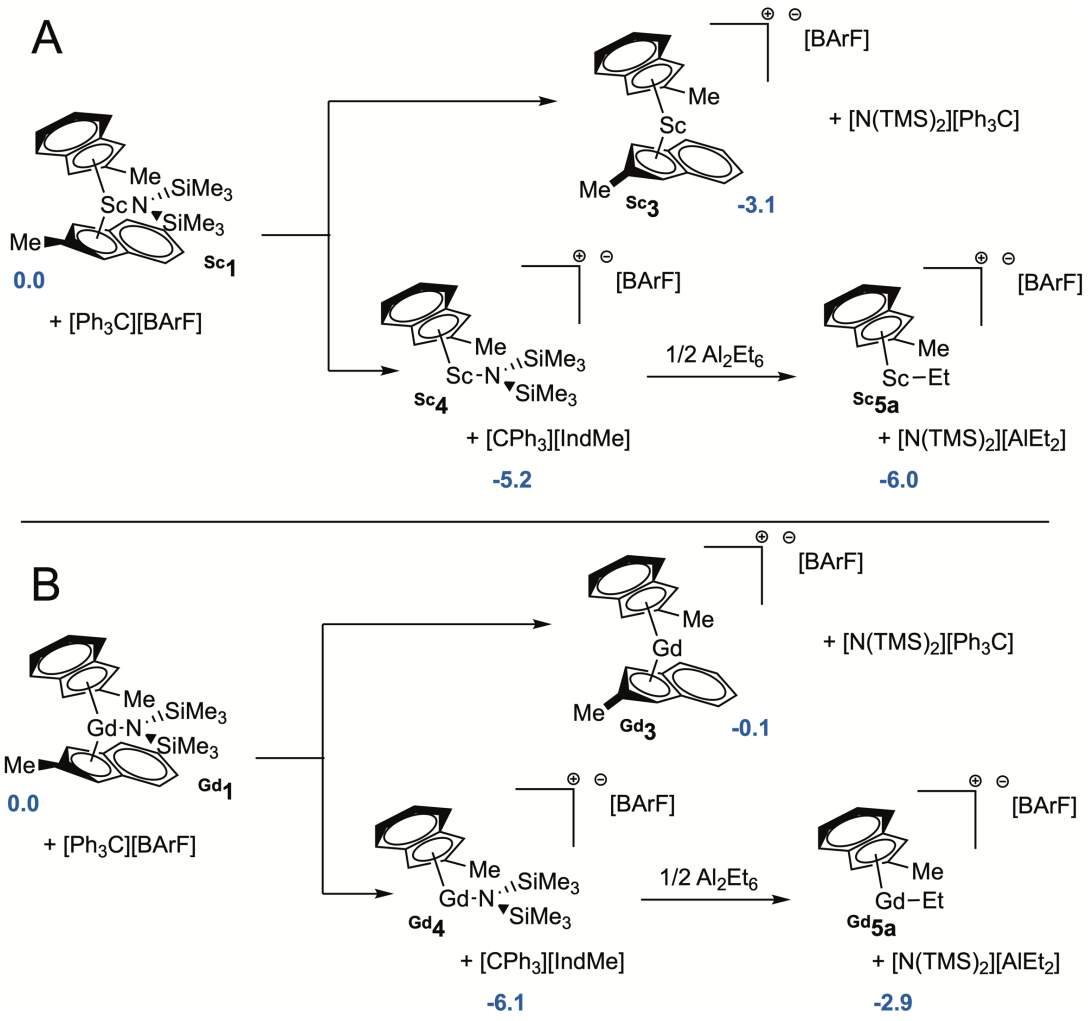

Scheme 6. Speciation of the ternary system ^{Sc}**1** (A) or ^{Gd}**1** (B) / [CPh$_3$][BArF] / TEA, [BArF]= [B(C$_6$F$_5$)$_4$], relative Gibbs energies in kcal mol^{-1}. All equilibriums considered are presented in the Scheme S1 and S5, only the most relevants are depicted in Scheme 6.

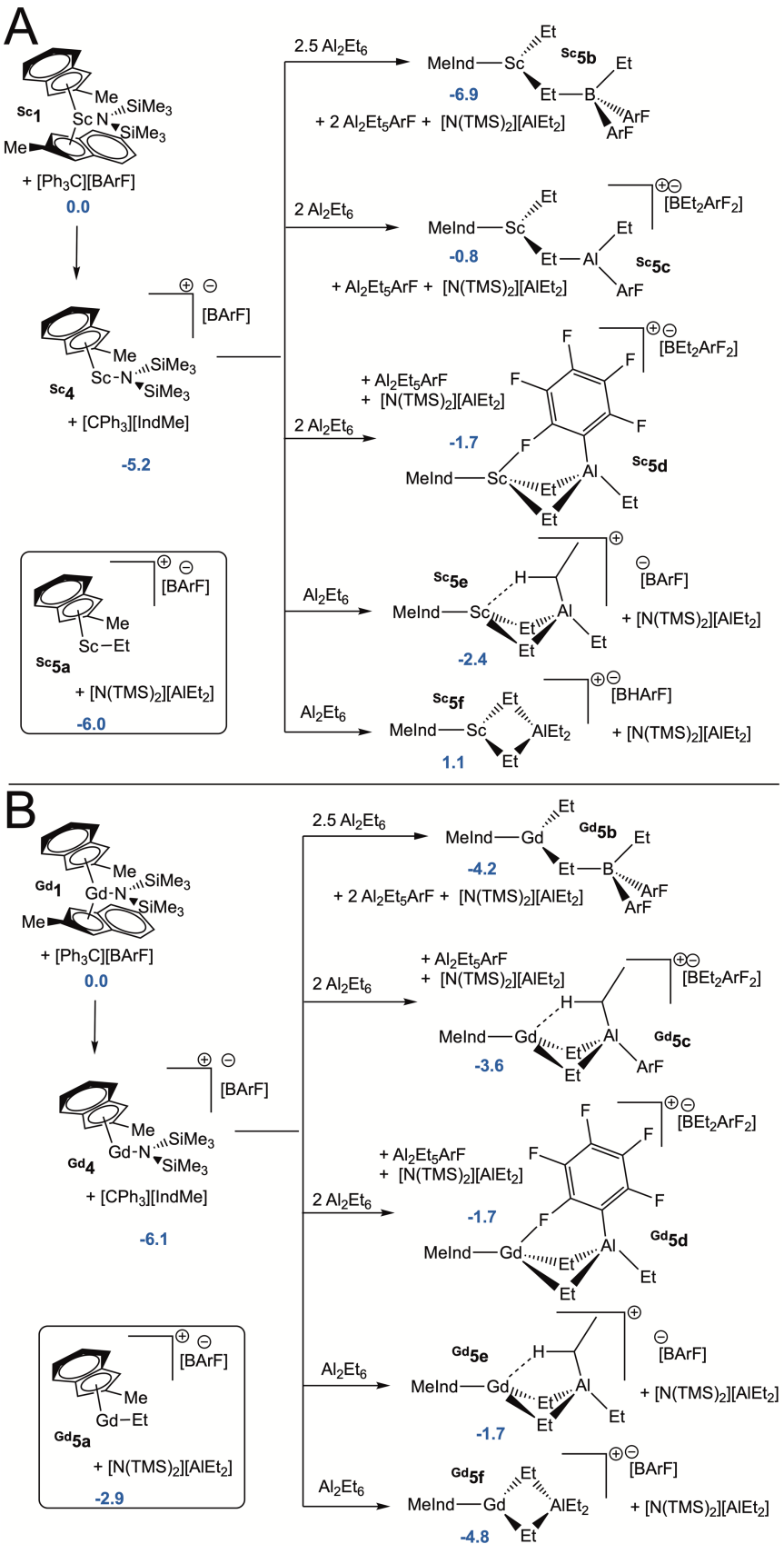
A
Sc1
+ [Ph3C][BArF]
0.0
Sc4
+ [CPh3][IndMe]
-5.2
Sc5a
+ [N(TMS)2][AlEt2]
-6.0
2.5 Al2Et6
Sc5b
-6.9
+ 2 Al2Et5ArF + [N(TMS)2][AlEt2]
2 Al2Et6
Sc5c
-0.8
+ Al2Et5ArF + [N(TMS)2][AlEt2]
2 Al2Et6
Sc5d
-1.7
+ Al2Et5ArF
+ [N(TMS)2][AlEt2]
Al2Et6
Sc5e
-2.4
+ [N(TMS)2][AlEt2]
Al2Et6
Sc5f
1.1
+ [N(TMS)2][AlEt2]
B
Gd1
+ [Ph3C][BArF]
0.0
Gd4
+ [CPh3][IndMe]
-6.1
Gd5a
+ [N(TMS)2][AlEt2]
-2.9
2.5 Al2Et6
Gd5b
-4.2
+ 2 Al2Et5ArF + [N(TMS)2][AlEt2]
2 Al2Et6
Gd5c
-3.6
+ Al2Et5ArF
+ [N(TMS)2][AlEt2]
2 Al2Et6
Gd5d
-1.7
+ Al2Et5ArF
+ [N(TMS)2][AlEt2]
Al2Et6
Gd5e
-1.7
+ [N(TMS)2][AlEt2]
Al2Et6
Gd5f
-4.8
+ [N(TMS)2][AlEt2]

Scheme 7. Speciation of the most relevant polymetallic species (**^{M}5b-f**, M = Sc panel A or Gd panel B) and their relative Gibbs energy in kcal mol^{-1}, [BArF] = [B(C$_6$F$_5$)$_4$], monometallic species **^{M}5a** (M = Sc or Gd) is quoted for comparison. All the polymetallic species, their associated equilibria and relative energies are available in the Scheme S3 and S6.

In order to complement the speciation, the putative formation polymetallic species with TEA and or [BArF] have been considered.[10,11] Experimentally, one equivalent of [CPh$_3$][BArF] is reported to react with the metallocene complex and the resulting mono-indenyl cation is reported to be contacted with four equivalents of TEA.[6] The equilibrium between the remaining borate counter-anion and TEA is illustrated by equation Eq. 1. This transmetalation reaction is exergonic by 2.4 kcal mol^{-1}.

$$[B(C_6F_5)_4]^- + 2\ Al_2Et_6 \quad = \quad [BEt_2(C_6F_5)_2]^- + 2\ Al_2Et_5(C_6F_5) \qquad (1)$$

Unfortunately, we were unable to properly converge transitions states for this reaction, its mechanism could not be determined. However, as this reaction shares similarities with some transmetalation reactions proceeding experimentally under mild conditions,[12] we have assumed that this transmetalation reaction is not kinetically limited and takes place based on its exergonicity.

The same speciation study has been conducted if the cationization is made with the [PhNHMe$_2$][BArF] salt (see Scheme S1, S4). Concerning Sc-based complexes, the cationization by the anilinium salt does not change the speciation: the most stable monometallic complex remains **^{Sc}5a** whose formation is exergonic by 5.1 kcal mol^{-1}, and the most stable bimetallic species

remains ^{Sc}**5b** whose formation is exergonic by 10.5 kcal mol^{-1}. It appears worth mentioning that the coordination of aniline to the metal center of cationic complex does not bring significant stabilization as this reaction is always computed thermoneutral.

In the case of Gd-based complexes, both cationizing agents led the same speciation. The most stable monometallic cationic complex is similar to ^{Sc}**5a**, the formation of this complex is slightly exergonic by 2.9 kcal mol^{-1} (see Scheme 6 and S5). In other words, alkylation of the Gd precursor is apparently less favorable than the alkylation of the Sc precursor by 4.2 kcal mol^{-1}, in presence of the counter-ion, accordingly to the isodesmic equation Eq. 2.

$$[(Ind')ScN(TMS)_2][BArF] + [(Ind')GdEt][BArF] = [(Ind')ScEt][BArF] + [(Ind')GdN(TMS)_2][BArF] \quad (2)$$

The same thermodynamic balance has been computed in absence of the [BArF] counter-ion. In this case, the reaction is almost thermoneutral. Thus, the differential binding interactions within the ion pair accounts for this difference. For gadolinium-based complexes, the most stable bimetallic species are analogs to **5b-e**. Relative to the gadolinium bis(indenyl) amido precursor ^{Gd}**1**, their formation is exergonic by 1.4 to 4.8 kcal mol^{-1} and are most likely present in mixture and in equilibria in the reaction media (see Scheme 7 and S6, S7). Thereof, regarding the study of the initiation of the butadiene polymerization, for both metals, all possible mode of insertion of butadiene in the monometallic ^{M}**5a** complex were evaluated, but also in bimetallic complexes ^{M}**5b-f** (M = Sc, Gd). Experimentally, Tardif et al. obtained a high proportion, close to 99%, of *cis*-1,4-polybutadiene. The reactivity of these different active sites has been studied to understand catalyst

selectivity. However, concerning the modelling of propagation steps, the reactivity of both 2-vinyl-alkyl and allyl sites were explored.

Before raising the interest on the selectivity of butadiene polymerization, we have first assessed and compared the reactivity metal-alkyl bonds in complexes ^{Sc}**5a-e**. For Sc-based complex ^{Sc}**5a**, the lowest transition state corresponds to the insertion of *trans*-butadiene. Relative to ^{Sc}**5a** and *trans*-butadiene, this barrier has been computed to 15.6 kcal mol^{-1}, whereas insertion of *cis*-butadiene requires 6.7 kcal mol^{-1} more and is thus unlikely (Table 1 and S1). Hence, after alkylation of the Sc catalyst, initiation specifically yields *syn*-allyl ^{ScT}**B**. For the bimetallic Sc / B complex ^{Sc}**5b**, transition state for butadiene insertion in all metal-carbon bonds has been tested. The lowest energy transition state is for *trans*-butadiene insertion in the Sc-Et terminal bond. This transition state is at 10.5 kcal mol^{-1} above ^{Sc}**5b** and *trans*-butadiene. Insertion of *cis*-butadiene requires less a kcal mol^{-1} more and appears kinetically competitive. Alternatives insertion mode requires either more than 30 kcal mol^{-1} or led to the dissociation of the Sc / B bimetallic complex such as for Sc / Al bimetallic complexes (Tables 1 and S1). Hence, relative to the common energy reference made of ^{Sc}**1** and its associated reactants, ^{Sc}**5b** preferentially initiates polymerization and yields a *syn*-allyl ^{ScT}**B** site. We have then considered the selectivity of the second butadiene insertion in a *syn*-allyl ^{ScT}**B** site. In this case, insertion of *cis*-butadiene to yield an *anti*-allyl ^{ScC}**B** site is kinetically favored as indicated by a difference in transition state Gibbs energy of 5.3 kcal mol^{-1} (Tables 1 and S2). At this stage we can conclude that polymer chain will start by a *trans*-butadiene unit, specifically followed by a *cis*-butadiene unit.

Table 1. Gibbs energy barriers and thermodynamics for the first insertion of butadiene depending on the active species and the metal center.

active species	$\Delta G^{\neq a}$ (kcal mol^{-1})		$\Delta_r G^{\circ a}$ (kcal mol^{-1})	
^{Sc}**5a**	^{ScC}***Bl****°	22.3	^{ScC}**Bl°**	-6.6
	^{ScT}***Bl****°	15.6	^{ScT}**Bl°**	-11.7
^{Sc}**5b**	^{ScC}***Br****°	11.4	^{ScC}**Br°**	-13.5
	^{ScT}***Bl****°	10.5	^{ScT}**Bl°**	-31.7
^{Gd}**5a**	^{GdC}***Bl****°	16.9	^{GdC}**Bl°**	-14.2
	^{GdT}***Br****°	16.2	^{GdT}**Br°**	-24.1
^{Gd}**5b**	^{GdC}***Br****°	8.6	^{GdC}**Br°**	-20.0
	^{GdT}***Br****°	8.4	^{GdT}**Br°**	-31.7

[a] Gibbs energy difference relative to the most stable complex (i.e. $^{Sc/Gd}$**5b**).

The reactivity of Gd-based bimetallic complexes has been explored as well. Regarding ^{Gd}**5b**, the most reactive bond is the terminal Gd-Et one in which *trans*-butadiene insertion requires to overcome an energy barrier of 8.4 kcal mol^{-1} relative to ^{Gd}**5b** and *trans*-butadiene; the similar insertion of *cis*-butadiene only requires 0.2 kcal mol^{-1} more. These insertions are ca. 6 kcal mol^{-1} lower in energy than the lowest energy barrier for butadiene insertion in the cationic ^{Gd}**5a**. Regarding Gd / Al bimetallic, attempts to optimize transition states for butadiene insertion are not systematically dissociative like for Sc / Al bimetallic complexes but requires at 30 kcal mol^{-1} to proceed and can thus be discarded (Table 1 and S6). As a result, ^{Gd}**5b** accounts for the initiation of the butadiene polymerization without selectivity regarding stereochemistry of the inserted unit. As for the Sc-based system, we have considered the second insertion of butadiene in a the *syn*-

allyl ^{GdT}**B**. The 2.5 kcal mol^{-1} difference in Gibbs energy barriers between *cis*- and *trans*-insertion of butadiene accounts for a high selectivity towards the formation an *anti*-allyl site. Hence, for the Gd-based systems, the first unit of butadiene is either *cis* or *trans*, whereas the second one is selectively *cis* (Table 1 and S7).

Butadiene homopolymerization reactivity landscape.

Energy profile without counter-ion. Although the affinity of [BArF]$^-$ towards metal allyl complexes [(Ind')M(η^3-C_4H_6-Et)]$^+$ (M = Sc, Gd) is computed in the order of 20 to 25 kcal mol^{-1}, in a first assumption, we have considered that the ion pair is dissociated during the steady state of the polymerization. Thus, propagation steps have been examined starting from *anti*-allyl ^{ScC}**B** which is taken as an energy reference. The computed more favorable free energy profile for butadiene insertions is shown in Figure 2.A. For clarity, only the lowest activation energies have been reported, alternative possibilities are given in the ESI, Scheme S8 and Tables S3 and S8. In general, insertions on the left side *l i.e.* on the opposite side of the indenyl substituent as illustrated in Scheme 4, are kinetically more favorable than insertions taking place on the right *r* side. Starting from active site ^{ScC}**B**, the η^3 coordination of *cis*-1,4 butadiene corresponds to the formation of the most stable adduct ^{Sc14C}**B**_^{C}**B*****l***. This coordination step is exergonic by 6.4 kcal mol^{-1}. The subsequent insertion via transition states ^{Sc14C}**B**^{C}**B*****l****** is associated to the smallest Gibbs energy barrier of 4.5 kcal mol^{-1} relative to the adduct. This step is thus barrierless relative to separated ^{ScC}**B** and *trans*-butadiene. In contrast, the insertion of *trans*-1,4 butadiene requires 9.5 kcal mol^{-1} to proceed *via* transition state ^{Sc14C}**B**^{T}**B*****l****** and relative to the adduct ^{Sc14C}**B**_^{T}**B*****l*** (Figure 2.A).

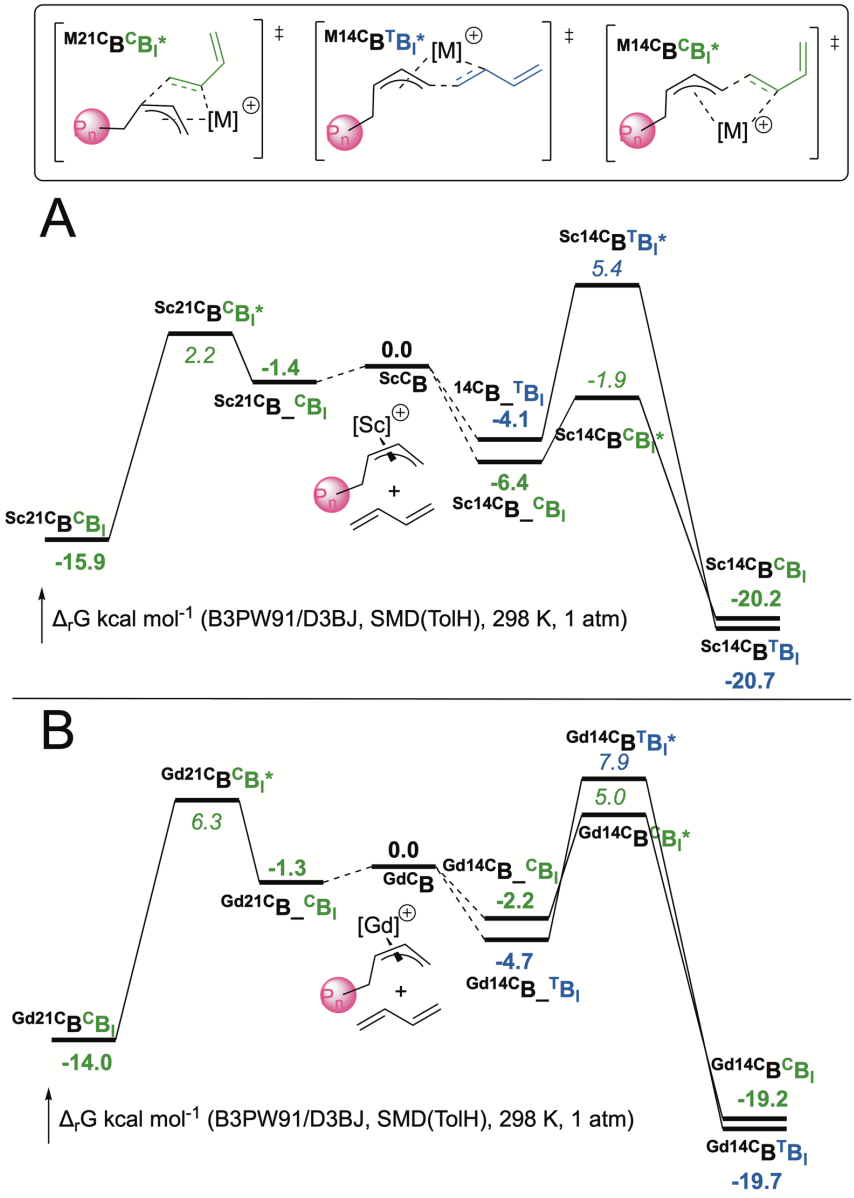

Figure 2. Gibbs free energy profile for the butadiene homopolymerization catalyzed by cationic scandium (A) and gadolinium (B) complexes ^{MC}**B** (M = Sc, Gd). P_n = Et. Energies referring to kinetics are in italic, energies referring to thermodynamics are in bold. $[M]^+$ accounts for 2-Me-Ind-metal cationic fragment (M = Sc, Gd). All the explored possibilities / conformers are available in see Tables S3 and S8.

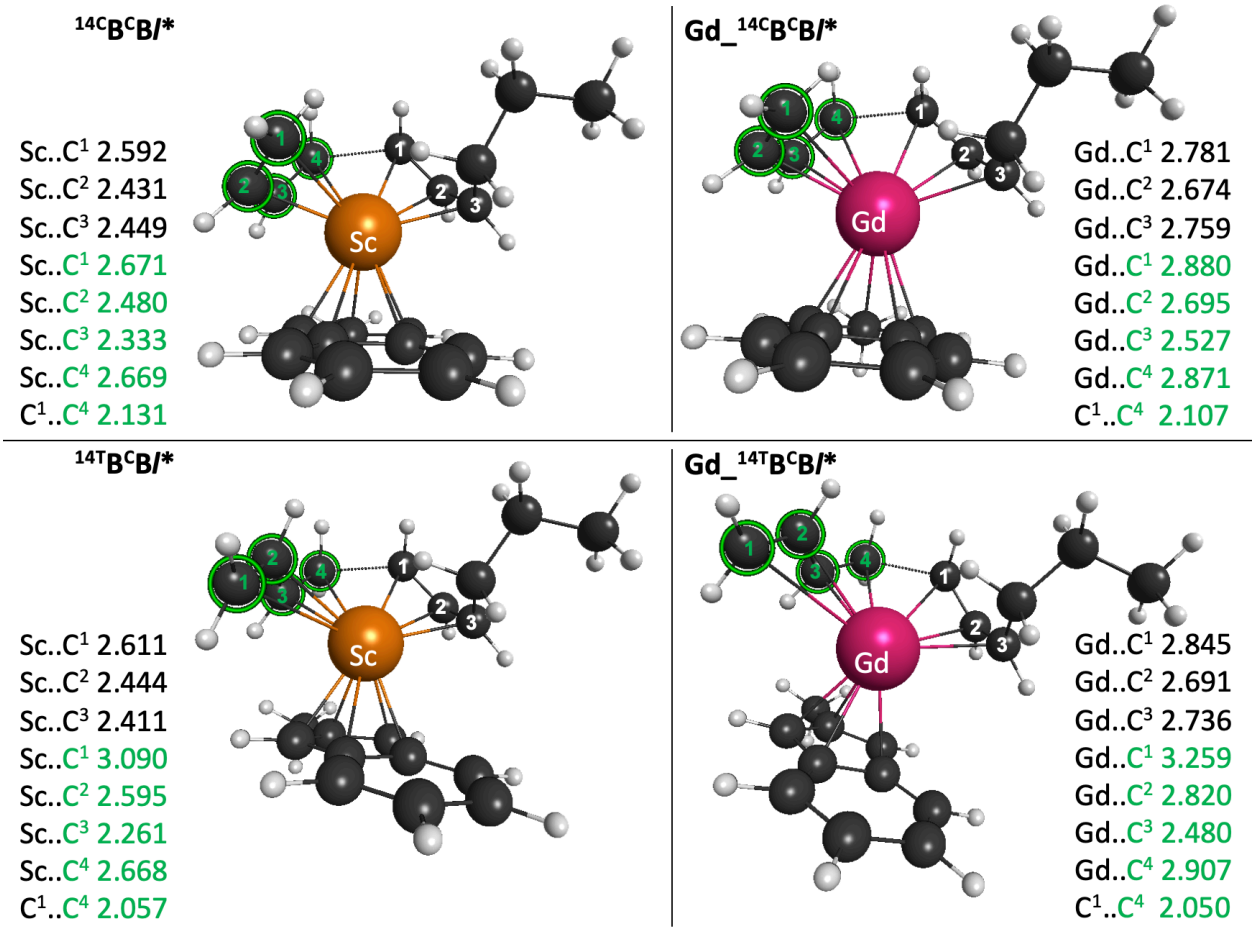

Figure 3. 3D representation of transition states ^{Sc14C}**B**^{C}**B***I****, ^{Sc14T}**B**^{C}**B***I****, ^{Gd14C}**B**^{C}**B***I**** and ^{Gd14T}**B**^{C}**B***I****. Key metal carbon and coupling C···C bond distances are given in Å. Inserted butadiene monomer is highlighted in green.

As 12% of 1,2-vinyl unit were characterized within the microstructure of the polymer, the energy profile associated to this sequence was computed as shown in Figure 2.A. The energy barrier between *cis*-2,1 adduct of butadiene ^{Sc21C}**B**_^{C}**B***I* and the subsequent insertion transition state ^{Sc21C}**B**^{C}**B***I**** is relatively low in energy 3.6 kcal mol^{-1}, but this transition state remains roughly 4 kcal mol^{-1} higher that the transition state ^{Sc14C}**B**^{C}**B***I****. This energy difference is in fair agreement

with the small amount of 1,2-vinyl unit, and thus supports the elusive 1,4 insertion of *trans*-butadiene whose transition state is even higher in energy.

Similar trends were obtained for the Gd-based complex. For this metal, relative to separated ^{GdC}**B** and *trans*-butadiene the lowest energy transition state ^{Gd14C}**B**^{C}**B*****l**** is at 5.0 kcal mol^{-1}, ^{Gd14C}**B**^{T}**B*****l**** is at 7.9 kcal mol^{-1} and ^{Gd21C}**B**^{C}**B*****l**** is at 16.1 kcal mol^{-1} (Figure 2.B). These values traduce the enhanced activity of the Sc based-system and the higher specificity towards 1,4 insertion for the Gd-based system, in line with experimental results. However, the computed *cis*-1,4 vs the *trans*-1,4 selectivity mismatches experimental data. This discrepancy may originate from the omission of the counter-ion in the chemical model. For that purpose, we have re-investigated the mechanism while explicitly including [BArF]$^{-}$ as a counter-ion as presented in the next section.

In order to relate the energetics of the computed energy profiles and especially the differences between Sc- and Gd-based systems, to the molecular structure of key transition states, Figure 3 displays transition states ^{M14C}**B**^{C}**B*****l**** and ^{M14C}**B**^{T}**B*****l**** (M = Sc, Gd) for Sc-based complexes and their Gd-based analogs. For both metals, the *cis* conformation of the inserted monomer allows a η^4 binding mode to the metal, whereas the *trans* conformation is better described by a η^3 binding mode as the M..C^{1}(butadiene) distance is raised by ca. 0.4 Å between these two isomers. This can be related to the better interaction with the metal that favors the binding and the insertion of the monomer.

Energy profile with the counter-ion. In order to evaluate the influence of the counter-ion on the reactivity of 2-vinyl-alkyle and allyl sites, structures have been re-optimized while explicitly taking the ion paring into account in the chemical model. Preliminary calculations revealed that, if a molecular interaction is characterized between the counter-ion and the metal complex, it is

between a fluorine atom of the fluoroarene and the metal center. Hence, in order to avoid additional sampling, $[Et_2B(C_6F_5)_2]^-$ has been represented by $[BArF]^-$ in the following.

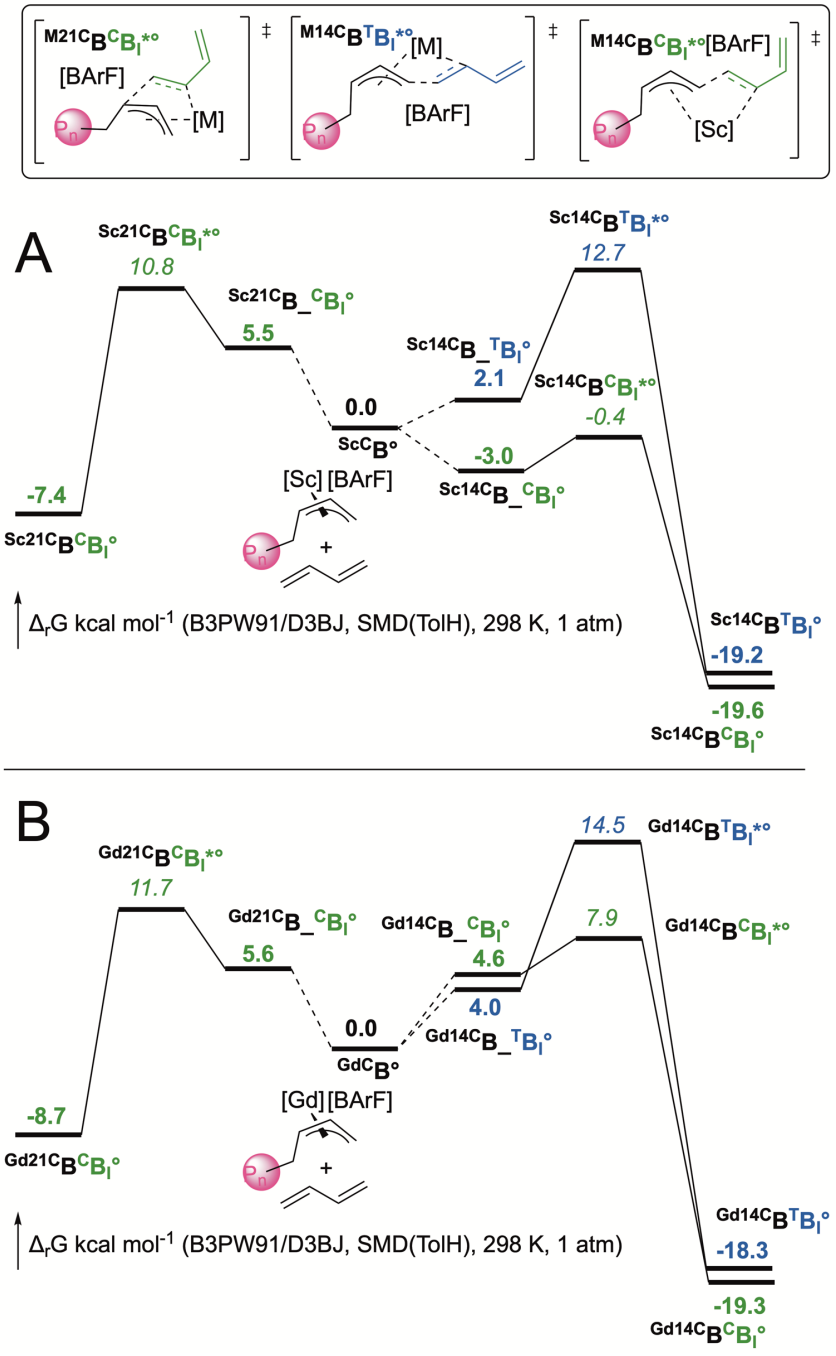

Figure 4. Gibbs free energy profile for the butadiene homopolymerization catalyzed by scandium (A) and gadolinium (B) ion-paired neutral complexes ^{MC}**B** (M = Sc, Gd) in presence of [BArF] as a counter-ion. P_n = Et. Energies referring to kinetics are in italic, energies referring to

thermodynamics are in bold. [Sc] accounts for 2-Me-Ind-Sc cationic fragment. All the explored possibilities / conformers are available in see Tables S5 and S10. As notation, ° refers to neutral catalytic complex.

Concerning Sc-based complexes, selectivity trends for butadiene insertions are similar to those previously discussed without the counter-ion. The *cis*-1,4 insertion of butadiene via transition state $^{Sc14C}\mathbf{B}^{C}\mathbf{B}\boldsymbol{I}^{*\circ}$ is associated to a Gibbs energy barrier of 2.6 kcal mol^{-1} relative to adduct $^{Sc14C}\mathbf{B\_}^{C}\mathbf{B}\boldsymbol{I}^{\circ}$ whose formation is exergonic by 3.0 kcal mol^{-1} as shown in Figure 4. Hence, even in the presence of the counter-ion, insertion of *cis*-butadiene into an *anti*-allyl is barrierless relative to an *anti*-allyl site. Thereof, the proximity of the counter-ion is not detrimental for the catalytic activity and selectivity. The relative energy of transition states $^{Sc14C}\mathbf{B}^{T}\mathbf{B}\boldsymbol{I}^{*\circ}$ and $^{Sc12C}\mathbf{B}^{C}\mathbf{B}\boldsymbol{I}^{*\circ}$ are still in agreement with the high specify of the catalyst in good agreement with experiment data.

Regarding the Gd-based system, the trends depicted above remain true but the presence of the counter-ion significantly modulates catalyst selectivities. For this metal, the lowest energy transition state $^{Gd14C}\mathbf{B}^{C}\mathbf{B}\boldsymbol{I}^{*\circ}$ is at 7.9 kcal mol^{-1}, $^{Gd14C}\mathbf{B}^{T}\mathbf{B}\boldsymbol{I}^{*}$ is at 14.5 kcal mol^{-1} and $^{Gd21C}\mathbf{B}^{C}\mathbf{B}\boldsymbol{I}^{*}$ is at 11.7 kcal mol^{-1} relative to separated $^{Gd14C}\mathbf{B}$ or $^{Gd21C}\mathbf{B}$ and *trans*-butadiene (see Table S10). Compared to the less realistic model in which the counter-ion is not considered, the lowest energy barrier associated to insertion of *cis*-butadiene in *anti*-allyl is raised by ca. 3 kcal mol^{-1}. More interestingly, the difference in transition state energies between insertions of *cis* and *trans* of butadiene is raised by 3.7 kcal mol^{-1} by explicitly adding the counter-ion. Thus, the counter-ion thus accounts for the quasi-specificity of the Gd-based system towards *cis*-1,4 polymerization. Similarly, the difference in energy between $^{Gd14C}\mathbf{B}^{C}\mathbf{B}\boldsymbol{I}^{*\circ}$ and $^{Gd21C}\mathbf{B}^{C}\mathbf{B}\boldsymbol{I}^{*\circ}$ is raised to almost 4 kcal mol^{-1} that also traduce a quasi-specificity of 1,4- over 2,1-insertions, as characterized experimentally.[6]

Geometry analyses along the reaction path show some interesting feature. In both ^{MC}**B** (M = Sc, Gd) four fluorine atoms are close to the metal center with, for example, distances ranging from 3.64 to 4.21 Å for ^{ScC}**B**. The η^4-coordination of butadiene induces a reorganization of the ion pair. In ^{Sc14C}**B**_^{C}**B*I*°**, only two Sc..F interactions are present with slightly elongated distances of 4.46 and 5.13 Å. This structure displays additional weak interactions between CH bonds of the allyl group pointing towards one ArF ring of the counter ion. These interactions are maintained at the transition states ^{Sc14C}**B**_^{C}**B*I**°** without displaying any significant interaction. This is in line with a recent experimental kinetic study on olefin insertion in metal-carbon of metallocenium ion-pair aggregates.[47]

Ethylene-Butadiene copolymerization reactivity landscape. The homopolymerization of ethylene and butadiene classically requires different conditions, performing the statistical copolymerization of these two monomers remains thus a challenge in the community.[1] Thus, the ability of the cationic catalytic systems depicted above to copolymerize ethylene with butadiene has been assessed computationally. In order to enlarge the discussion, copolymerization energy profiles have also been computed for the neutral bis-indenyl Sc- and Gd-based complexes. Gibbs energy barriers are then compared to those of the neutral bis-fluorenyl Nd-based[27] system that is known to copolymerize efficiently ethylene with butadiene.[48,49,50]

In order to perform the statistical copolymerization of ethylene with butadiene, we have shown that one critical criterion is the energy barrier for ethylene insertion in an allyl site (**BE***) relative to the one of butadiene in the same site (**BB***).[27] For both Sc- and Gd-based cationic systems, in absence of the counter-ion, insertion of ethylene into an allyl site (**BE***) requires at least 10 kcal mol^{-1} more than insertion of butadiene into the same site (**BB***) (Table 2). Additionally, the insertion of ethylene into an alkyl site (**EE***) requires at least 2 kcal mol^{-1} more than the insertion

of *cis*-butadiene (**EB***). Thereof, the electrophilicity of both Sc and Gd-based cationic complexes prevail binding and insertion of butadiene. over ethylene These catalytic systems are thus not expected to yield ethylene-butadiene statistical copolymers under copolymerization conditions. However, the group of Hou as reported both statistical and alternating copolymerization of isoprene with ethylene mediated by cationic half-sandwich scandium alkyl camplexes.[51] For these catalytic systems, the activity and the selectivity proved to be significantly dependent on structure and nature of the ancillary ligand.[51] The exhaustive mechanistic investigation of the ethylene / butadiene copolymerization reaction is available in Tables S3, S4, S8, S9, S11 to S14.

Table 2. Gibbs energy barrier in kcal mol^{-1} characteristic of the ethylene / butadiene copolymerization.

insertion sequence	$[Sc]^{+}$ [a]	$[Gd]^{+}$ [a]	[Sc]° [b]	[Gd]° [b]	[Nd]° [c] [34]
BE*	14.9	19.6	14.7	25.3	15.8
BB*	4.5 *anti* [d]	6.7 *anti* [d]	15.8 *anti* [d]	21.8 *alkyl* [d]	24.9 *syn* [d]
EE*	8.3	14.4	13.8	15.8	22.6
EB*	6.5 *anti* [d]	7.6 *syn* [d]	17.8 *syn* [d]	13.4 *syn* [d]	22.6 *syn* [d]

[a]complexes $[Ind'MR]^{+}$ (R = alkyl or allyl) computed without the counter-ion; [b]neutral complexes [*anti*-Ind'_2MR] (R = alkyl or allyl); [c]neutral system $[Me_2Si(C_{13}H_8)_2NdR]$ / R_2Mg. [d]allyl conformation yielded.

In order to highlight the effect of cationization, copolymerization energy profiles have been computed for the neutral system [Ind'_2MR] (M = Sc, Gd; R= alkyl or allyl site). In this case, energy barriers for butadiene insertions in allyl or alkyl are significantly raised and are thus more balanced with energy barriers for ethylene insertions. For example, the difference in energy barrier between

ethylene and butadiene insertions into an *anti*-allyl site (**BE*** vs **BB***) does not exceed a 1 kcal mol^{-1} for [Sc]° (resp. 4 kcal mol^{-1} for [Gd]°). Furthermore, for the neutral Gd based complex [Ind'$_2$GdR], insertion barriers are comparable to those computed for the bis-fluorenyl Nd-based complex.[27] For the neutral Sc based complex, analogous insertion barriers are lower (Table 2).

These trends suggest that neutral catalytic systems are more suited than cationic ones to perform the statistical or alternating copolymerization of ethylene with butadiene but with a lesser global activity. However, for cationic systems, as the energy barrier for ethylene insertion remains accessible, formation of ethylene rich sequences appears manageable if the concentration of diene drops, as observed the group of Cui for thiophene-fused cyclopentadiene-ligated scandium based catalytic systems,[52] and patented as well.[53]

Finally, for neutral catalytic systems, several transition isomers are within a 3 kcal mol^{-1} (see Table S11, S12, S13 and S14). As reported for Nd- and Zr-based complexes,[1] a large diversity of microstructure is awaited upon fine tuning of the ligand and counter-ion structures as well as reaction conditions.

CONCLUSION

In this study, the speciation and the reactivity of cationic Sc and Gd d^0 metal complexes for the butadiene homopolymerization has been achieved at the DFT level. The formation of a dormant multicomponent catalytic system is highlighted. The presence of the cationic agent and the alkylating agent leads to a mixture of several cationic mono- and polymetallic species. Consequently, it is mandatory to take all plausible species into account. Likewise, the counter-ion of these cationic catalytic systems can significantly affect both the activity and the selectivity of the catalytic systems. In this study, in which the counter-ion has been both omitted and added to

the chemical model, we have demonstrated that the counter-ion enhances the activity of the Sc-based system and raise the selectivity towards *cis*-insertion of the Gd based system. The explicit modelling of ion pairing allowed us to alleviate discrepancies between experimental and computed trends. Finally, regarding the copolymerization of ethylene with butadiene, by comparison with the characteristic energy profile of neutral Nd-based catalytic systems, we demonstrate that cationic Sc and Gd complexes cannot perform such copolymerization due to its lack of affinity towards ethylene if butadiene is also available in the reaction media. Alternatively, neutral Sc and Gd complexes which might be potential candidate for ethylene-butadiene copolymerization.

ASSOCIATED CONTENT

Supporting Information. Supporting energy profiles and additional structural sampling are provided as a supplementary material, as well as all the Cartesian coordinates and associated computed energies. The following files are available free of charge.

AUTHOR INFORMATION

Corresponding Authors

* e-mail for L.P.: lionel.perrin@univ-lyon1.fr

* e-mail for M.-N.P.: marie-noelle.poradowski@michelin.com

Author Contributions

The manuscript was written through contributions of all authors. All authors have given approval to the final version of the manuscript.

Funding Sources

L.V., M.-N.P. and L.P. thank Manufacture Michelin for financial support. L.P thanks the CNRS and le Ministère de l'Enseignement Supérieur et de la Recherche (MESR) for funding.

Notes

The authors declare no competing financial interest.

ACKNOWLEDGMENT

L.V., M.-N.P. and L.P. thank CCIR facility of ICBMS and P2CHPD computer center of Université Lyon 1 for generous donations of computational time and technical support.

REFERENCES

(1) Belaid, I.; Monteil, V.; Boisson, C. Chapter n°18: Copolymerization of Ethylene with Conjugated Dienes, in *Handbook of Transition Metal Polymerization Catalysts* (Ed. R. Hoff), 2018, 661–692.

(2) Sauter, D. W.; Taoufik, M.; Boisson, C. Polyolefins, a Success Story *Polymers* **2017**, *9*, 185–198.

(3) Friebe, L.; Nuyken, O.; Obrecht, W. Neodymium Based Ziegler Catalysts – Fundamental Chemistry, in *Adv. Polym. Sci.* (Ed. O. Nuyken), 2006, 204, 1–154.

(4) Forens, A.; Roos, K.; Dire, C.; Gadenne, B.; Carlotti, S. Accessible microstructures of polybutadiene by anionic polymerization. *Polymer* **2018**, 153, 103–122.

(5) Gaioto, C. C.; Schmal, M.; da Silva Pinto, J. Neodymium versatate catalyst for the 1,3-butadiene polymerization – Effects of reaction parameters. *Catal. Today* **2020**, *344*, 84–91.

(6) Tardif, O.; Kaita, S. Generation of cationic indenyl silylamide gadolinium and scandium complexes $[(Ind)Ln(N(SiMe_3)_2)]^+[B(C_6F_5)_4]^-$ and their reactivity for 1,3-butadiene polymerization. *Dalton Trans.* **2008**, *19*, 2531–2533.

(7) Kaita, S.; Hou, Z.; Nishiura, M.; Doi, Y.; Kurazumi, J.; Horiuchi, A. C.; Wakatsuki, Y. Ultimately Specific 1,4-cis Polymerization of 1,3-Butadiene with a Novel Gadolinium Catalyst. *Macromolecules Rapid Communication* **2003**, *24*, 179–184.

(8) Kaita, S.; Doi, Y.; Kaneko, K.; Horiuchi, A. C.; Wakatsuki, Y. An Efficient Gadolinium Metallocene-Based Catalyst for the Synthesis of Isoprene Rubber with Perfect 1,4-Cis Microstructure and Marked Reactivity Difference between Lanthanide Metallocenes toward Dienes As Probed by Butadiene−Isoprene Copolymerization Catalysis. *Macromolecules* **2004**, *37*, 5860–5862.

(9) Kaita, S.; Hou, Z.; Wakatsuki, Y. Stereospecific Polymerization of 1,3-Butadiene with Samarocene-Based Catalysts. *Macromolecules* **1999**, *32*, 9078-9079.

(10) Ehm, C.; Cipullo, R.; Budzelaar, P. H. M.; Busico, V. Role(s) of TMA in polymerization. *Dalton Trans.* **2016**, *45*, 6847–6855.

(11) Parfenova, L. V.; Kovyazin, P. V.; Gabdrakhmanov, V. Z.; Istomina, G. P.; Ivchenko, P. V.; Nifant'Ev, I. E.; Dzhemilev, U. M. Ligand exchange processes in zirconocene dichloride-

trimethylaluminum bimetallic systems and their catalytic properties in reaction with alkenes. *Dalton Trans.* **2018**, *47*, 16918–16937.

(12) Mathis, D.; Couzijn, E. P. A.; Chen, P. Structure, dynamics, and polymerization activity of zirconocenium ion pairs generated with boron-C_6F_5 compounds and Al_2R_6. *Organometallics* **2011**, *30*, 3834–3843.

(13) Tensi, L.; Froese, R. D. J.; Kuhlman, R. L.; Macchioni, A.; Zuccaccia, C. Interception of Elusive Cationic Hf–Al and Hf–Zn HeterobimetallicAdducts with Mixed Alkyl Bridges Featuring Multiple Agostic Interactions. *Chem. Eur.–J.* **2020**, *26*, 3758–3766.

(14) Laine, A.; Coussens, B. B.; Hirvi, J. T.; Berthoud, A.; Friederichs, N.; Severn, J. R.; Linnolahti, M. Effect of Ligand Structure on Olefin Polymerization by a Metallocene/Borate Catalyst: A Computational Study. *Organometallics* **2015**, *34*, 2415–2421.

(15) Xu, Z.; Vanka, K.; Ziegler, T. The influence of the counter-ion $MeB(C_6F_5)_3^-$ and solvent effects on ethylene polymerization catalyzed by $[(CpSiMe_2NR)TiMe]^+$: A combined density functional theory and molecular mechanism study. *Macromol. Symp*. **2004**, *206*, 457–469.

(16) Vanka, K.; Chan, M. S. W.; Pye, C. C.; Ziegler, T. A Density Functional Study of Ion-Pair Formation and Dissociation in the Reaction between Boron- and Aluminum-Based Lewis Acids with $(1,2\text{-}Me_2Cp)_2ZrMe_2$. *Organometallics* **2000**, *19*, 1841–1849.

(17) Matsumoto, K.; Sandhya, K. S.; Takayanagi, M.; Koga, N.; Nagaoka, M. An Active Site Opening Mechanism in a (pyridylamide)hafnium(IV) Ion Pair Catalyst: An Associative Mechanism. *Organometallics* **2016**, *35*, 4099–4105.

(18) Titov, A.V.; Mosyagin, N. S. Generalized relativistic effective core potential: Theoretical grounds. *Int. J. Quantum Chem.* **1999**, *71*, 359–401.

(19) Maron, L.; Eisenstein, O. Do f Electrons Play a Role in the Lanthanide−Ligand Bonds? A DFT Study of $Ln(NR_2)_3$; R = H, SiH_3. *J. Phys. Chem. A* **2000**, *104*, 7140–7143.

(20) Dolg, M.; Stoll, H.; Savin, A.; Preuß, H. Energy-adjusted pseudopotentials for the rare earth elements. *Theor. Chim. Acta* **1989**, *75*, 173–194.

(21) Roca-Sabio, A.; Regueiro-Figueroa, M.; Esteban-Gomez, D.; De Blas, A.; Rodriguez-Blas, T.; Platas-Iglesias, C. Density functional dependence of molecular geometries in lanthanide(III) complexes relevant to bioanalytical and biomedical applications. *Comput. Theor. Chem.* **2012**, *999*, 93−104.

(22) Dolg, M.; Stoll, H.; Savin, A.; Preuß, H. Energy-adjusted pseudopotentials for the rare earth elements. *Theor. Chim. Acta* **1989**, *75*, 173–194.

(23) Dolg, M.; Stoll, H.; Savin, A.; Preuss, H. A combination of quasirelativistic pseudopotential and ligand field calculations for lanthanoid compounds. *Theor. Chim. Acta* **1993**, *85*, 441–450.

(24) Bergner, A.; Dolg, M.; Küchle, W.; Stoll, H.; Preuß, H. Ab initio energy-adjusted pseudopotentials for elements of groups 13-17. *Mol. Phys.* **1993**, *80*, 1431–1441.

(25) Krishnan, R.; Binkley, J.; Seeger, R.; Pople, J. Self-consistent molecular orbital methods. XX. A basis set for correlated wave functions. *J. Chem. Phys.* **1980**, *72*, 650–654.

(26) Clark, T.; Chandrasekhar, J.; Spitznagel, G.; Schleyer, P. Efficient diffuse function-augmented basis sets for anion calculations. III. The 3-21+G basis set for first-row elements, Li–F. *J. Comp. Chem.* **1983**, *4*, 294–301.

(27) Nsiri, H.; Belaid, I.; Larini, P.; Thuilliez, J.; Boisson, C.; Perrin, L. Ethylene-Butadiene Copolymerization by Neodymocene Complexes: A Ligand Structure / Activity / Polymer Microstructure Relationship Based on DFT Calculations. *ACS Catal.* **2016**, *6*, 1028–1036.

(28) Ehm, C.; Antinucci, G.; Budzelaar, P. H. M.; Busico, V. Catalyst activation and the dimerization energy of alkylaluminium compounds. *J. Organomet. Chem.* **2014**, *772-773*, 161–171.

(29) Becke, A. D. Density-functional thermochemistry. III. The role of exact exchange. *J. Chem. Phys.* **1993**, *98*, 5648–5652.

(30) Perdew, J. P.; Wang, Y. Accurate and simple analytic representation of the electron-gas correlation energy. *Phys. Rev. B* **1992**, *45*, 13244–13249.

(31) Kefalidis, C. E.; Castro, L.; Perrin, L; Del Rosal, I.; Maron, L. New perspectives in organolanthanide chemistry from redox to bond metathesis: Insights from theory. *Chem. Soc. Rev.* **2016**, *45*, 2516–2543.

(32) Perrin, L.; Bonnet, F.; Chenal, T.; Visseaux, M.; Maron, L. A DFT study of conjugated dienes polymerisation catalyzed by $[Cp^*ScR]^+$: Insights into the propensity for *cis*-1,4 insertion, *Chem.-Eur. J.* **2010**, *16*, 11376–11385.

(33) Perrin, L., Maron, L.; Eisenstein, O. Chemoselectivity in σ bond activation by lanthanocene complexes from a DFT perspective: Reactions of Cp_2LnR (R = CH_3, H, SiH_3) with SiH_4 and CH_3-SiH_3. *New J. Chem.* **2007**, *31*, 549–555.

(34) Marenich, A.; Cramer, C.; Truhlar, D. Universal solvation model based on solute electron density and on a continuum model of the solvent defined by the bulk dielectric constant and atomic surface tensions. *J. Phys. Chem. B* **2009**, *113*, 6378–6396.

(35) Castro, L.; Kirillov, E.; Miserque, O.; Welle, A.; Haspeslagh, L.; Carpentier, J.F.; Maron, L. Are Solvent and Dispersion Effects Crucial in Olefin Polymerization DFT Calculations? Some Insights from Propylene Coordination and Insertion Reactions with Group 3 and 4 Metallocenes. *ACS Catal.* **2015**, *5*, 416−425.

(36) Grimme, S.; Antony, J.; Ehrlich, S.; Krieg, H. A consistent and accurate ab initio parametrization of density functional dispersion correction (DFT-D) for the 94 elements H-Pu. *J. Chem. Phys.* **2010**, *132*, 154104.

(37) Grimme, S., Ehrlich, S. and Goerigk, L. Effect of the damping function in dispersion corrected density functional theory. *J. Comput. Chem.* **2011**, *32*, 1456–1465.

(38) Gaussian 09, Revision D.01, Frisch, M. J.; Trucks, G. W.; Schlegel, H. B.; Scuseria, G. E.; Robb, M. A.; Cheeseman, J. R.; Scalmani, G.; Barone, V.; Mennucci, B.; Petersson, G. A.; Nakatsuji, H.; Caricato, M.; Li, X.; Hratchian, H. P.; Izmaylov, A. F.; Bloino, J.; Zheng, G.; Sonnenberg, J. L.; Hada, M.; Ehara, M.; Toyota, K.; Fukuda, R.; Hasegawa, J.; Ishida, M.; Nakajima, T.; Honda, Y.; Kitao, O.; Nakai, H.; Vreven, T.; Montgomery, J. A., Jr.; Peralta, J. E.; Ogliaro, F.; Bearpark, M.; Heyd, J. J.; Brothers, E.; Kudin, K. N.; Staroverov, V. N.; Kobayashi, R.; Normand, J.; Raghavachari, K.; Rendell, A.; Burant, J. C.; Iyengar, S. S.; Tomasi, J.; Cossi, M.; Rega, N.; Millam, J. M.; Klene, M.; Knox, J. E.; Cross, J. B.; Bakken, V.; Adamo, C.; Jaramillo, J.; Gomperts, R.; Stratmann, R. E.; Yazyev, O.; Austin, A. J.; Cammi, R.; Pomelli, C.; Ochterski, J. W.; Martin, R. L.; Morokuma, K.; Zakrzewski, V. G.; Voth, G. A.; Salvador, P.;

Dannenberg, J. J.; Dapprich, S.; Daniels, A. D.; Farkas, Ö.; Foresman, J. B.; Ortiz, J. V.; Cioslowski, J.; Fox, D. J. Gaussian, Inc., Wallingford CT, 2009.

(39) Talarico, G.; Blok, A. N. J.; Woo, T. K.; Cavallo L. Comparison of ab initio and DFT methods for studying chain propagation and chain termination processes with group 4 polymerization catalysts. 1. The *ansa*-bis(cyclopentadienyl)zirconium catalyst. *Organometallics* **2002**, *21*, 4939−4949.

(40) Smith, M. B. The monomer-dimer equilibria of liquid aluminum alkyls II. Trisisobutylaluminum. *J. Organomet. Chem.* **1970**, *22*, 273–281.

(41) Yuan, Y.; Zuo, R.; Zhang, Z.; Mao, K.; Tang, L.; Liu, J.; Li, Z. Study on the reaction of trimethylaluminum dimer and ammonia based on density functional theory. *Comput. Theor. Chem.* **2018**, *1139*, 77–81.

(43) McGrady, G. S. Structure of the trimethylaluminum dimer as determined by powder neutron diffraction at low temperature. *Organometallics* **2000**, *19*, 4398–4401.

(43) Smith, M. B. Monomer-dimer equilibria of liquid aluminum alkyls. I. Triethylaluminum. *J. Phys. Chem.* **1967**, *71*, 2, 364–370.

(44) Vranka, R. G.; Amma, E. L. Crystal structure of trimethylaluminum. *J. Am. Chem. Soc.* **1967**, *89*, 3121–3126.

(45) McGrady, G. S.; Turner, J. F. C.; Ibberson, R. M.; Prager M. Structure of the Trimethylaluminum Dimer As Determined by Powder Neutron Diffraction at Low Temperature. *Organometallics* **2000**, 19, 4398–4401.

(46) Eisenstein, O.; Gérard, H. Structure, Bonding, and Reactivity of Organoaluminum Molecular Species: A Computational Perspective, in *PATAI'S Chemistry of Functional Groups* (Ed. Z. Rappoport), 2017, 1–32.

(47) Sian, L.; Macchioni, A.; Zuccaccia, C. Understanding the Role of Metallocenium Ion-Pair Aggregates on the Rate of Olefin Insertion into the Metal–Carbon Bond. *ACS Catal.* **2020**, *10*, 1591–1606.

(48) Monteil, V.; Spitz, R.; Barbotin, F.; Boisson, C. Evidence of Intramolecular Cyclization in Copolymerization of Ethylene with 1,3-Butadiene: Thermal Properties of the Resulting Copolymers. *Macromol. Chem. Phys.* **2004**, *205*, 737−742.

(49) Thuilliez, J.; Ricard, L.; Nief, F.; Boisson, F.; Boisson, C. *ansa*-Bis(fluorenyl)neodymium Catalysts for Cyclocopolymerization of Ethylene with Butadiene; *Macromolecules* **2009**, *42*, 3774−3779.

(50) Llauro, M. F.; Monnet, C.; Barbotin, F.; Monteil, V.; Spitz, R.; Boisson, C. Investigation of Ethylene/Butadiene Copolymers Microstructure by ^{1}H and ^{13}C NMR. *Macromolecules* **2001**, *34*, 6304−6311.

(51) Li, X.; Nishiura, M.; Hu, L.; Mori, K.; Hou, Z. J. Alternating and Random Copolymerization of Isoprene and Ethylene Catalyzed by Cationic Half-Sandwich Scandium Alkyls. *J. Am. Chem. Soc.* **2009**, *131*, 13870–13882.

(52) Wu, C.; Liu, B.; Lin, F.; Wang, M.; Cui. D. *cis*-1,4-Selective Copolymerization of Ethylene and Butadiene: A Compromise between Two Mechanisms. *Angew. Chem. Int. Ed.* **2017** *56*, 6975–6979.

(53) Patent EP 2 599 800A1.

GRAPHICAL TOC